applied sciences

MDPI

Article

Study on the Length of the Effective Vibration Area of the Catenary in a Pantograph–Catenary Interaction System

Liming Chen [1], Like Pan [1,*], Yan Xu [2] and Chengbin Huang [2]

[1] China Academy of Railway Sciences Co., Ltd., Beijing 100081, China; 13810305638@163.com
[2] Faculty of Transportation Engineering, Kunming University of Science and Technology, Kunming 650504, China; xuyanrailway@kust.edu.cn (Y.X.); huangchengbin422@163.com (C.H.)
* Correspondence: plk1986@126.com

Abstract: The effective vibration area includes most of the catenary vibration caused by pantograph–catenary interactions and is the basis of the real-time catenary model for hardware-in-the-loop simulation. However, while the length of the effective vibration area is one of the most important parameters of the real-time catenary model, it has not been fully studied at present. In this paper, the length of the effective vibration area is first investigated. A pantograph–catenary interaction model is developed based on the modal superposition method. After the validation of the model, the vibration energy distribution of the catenary is used to determine the length of the effective vibration area based on the converged total energy. The influence of vehicle velocity and contact wire tension on the vibration energy distribution and length of the effective vibration area is investigated. The obtained appropriate length of effective vibration area is validated by a real-time catenary model and online measurement data of the contact force. The investigation results show that the energy distribution of the catenary can accurately determine the length of effective vibration area, and it increases with increasing vehicle velocity but decreases with increasing contact wire tension. The appropriate length of effective vibration area should be at least 160 m (approximately three spans) in the pantograph–catenary system.

Keywords: pantograph–catenary interaction; effective vibration area; real-time catenary model; energy distribution

Citation: Chen, L.; Pan, L.; Xu, Y.; Huang, C. Study on the Length of the Effective Vibration Area of the Catenary in a Pantograph–Catenary Interaction System. *Appl. Sci.* **2024**, *14*, 6822. https://doi.org/10.3390/app14156822

Academic Editors: Ján Dižo, Alyona Lovska and Miroslav Blatnický

Received: 12 May 2024
Revised: 11 July 2024
Accepted: 12 July 2024
Published: 5 August 2024

1. Introduction

The pantograph–catenary system is one of the most important subsystems in electrified railways, and its working performance affects the working performance of the whole railway system. In the pantograph–catenary system, the pantograph–catenary interaction dynamics directly determine its working performance and poor pantograph–catenary interaction dynamics can cause different failures, including arcing [1] and abnormal wear of the contact strip [2]. The increasing train operation speed worsens the dynamic behavior of the pantograph–catenary interaction and threatens the working performance of the pantograph–catenary system [3,4]. To ensure the operation reliability of the pantograph–catenary system, it is necessary to investigate the dynamics of the pantograph–catenary interaction at present.

Many scholars have contributed to the investigation of pantograph–catenary interaction dynamics from different aspects [5–10]. Poetsch et al. [5] studied the pantograph–catenary interaction dynamics and its control methods in the early stage. Later, Zhang et al. [6] studied the influence of pre-sag and contact wire irregularity on pantograph interaction dynamics. Bocciolone et al. [7] further investigated the aerodynamics of the pantograph = catenary system. Gregori et al. [8] developed a finite element method-based method to efficiently solve the dynamic responses of the pantograph–catenary interaction. The pantograph–catenary interaction benchmark was developed by Bruni et al. [10].

The EN 50318-2018 standard [11] is also proposed based on existing investigation results as the standard of pantograph–catenary interaction simulation and experimental models. Recently, Song et al. [12] even used deep, long-short-term memory neural networks to efficiently investigate the dynamics of pantograph–catenary interactions. Traditionally, pantograph–catenary interactions are considered to influence all catenary structures, and the finite element method (FEM) [13–15] and modal superposition method (MSM) [16–18] are mainly used to model pantograph–catenary interactions with all catenary structures considered. However, the increasing train operation speed lets the pantograph continuously interact with a long catenary structure due to the long travel distance of the vehicle. With a long catenary model considered, the number of degrees of freedom (DOFs) of the whole pantograph–catenary interaction model is greatly increased, and its calculation efficiency is decreased. This is harmful to the investigation of pantograph–catenary long-term dynamic behavior and the development of pantograph–catenary hardware-in-loop simulations, where both calculation accuracy and efficiency are needed.

In 2012, Facchinetti and Bruni [18] found that the pantograph–catenary interaction does not influence the whole catenary structure and the vibration of the catenary caused by the pantograph–catenary interaction is mainly concentrated in a small area around the moving pantograph. This small area is the effective vibration area (EVA), as shown in Figure 1. Based on the EVA, they developed a real-time catenary model for a hardware-in-the-loop pantograph–catenary interaction simulation. In the real-time catenary model, the long catenary is reduced to EVA (3–5 spans) and modeled using the MSM. When the pantograph moves near the boundary of the real-time catenary model, the whole model moves forward to let the pantograph located in the center of the model again, and the initial condition of the model after movement is derived based on the calculation results of the model before movement. Because only the EVA (3–5 spans) instead of the whole long catenary (normally 20 spans) needs to be modeled, the number of DOFs of the whole model is greatly decreased, and its calculation efficiency is improved when calculating the dynamic responses of the pantograph–catenary interaction with a long catenary considered.

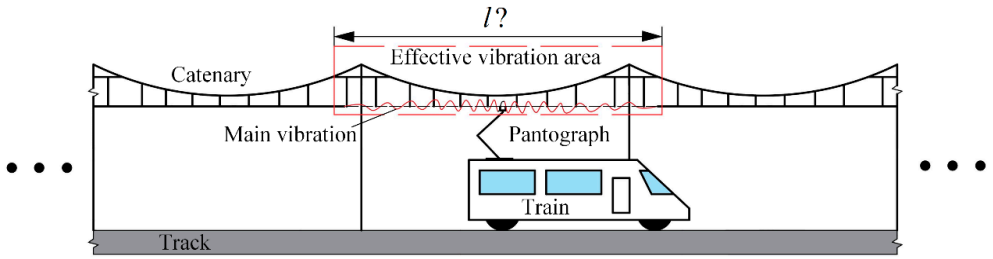

Figure 1. Schematic of the effective vibration area in the pantograph–catenary interaction.

Later, Bruni [19] and Facchinetti [20] further improved this model to formulate the hardware-in-the-loop pantograph–catenary interaction test bench. The same theory is also used in train-track interaction simulation models, such as the moving element model [21,22] and the reduced beam model [23,24]. These new methods have proved accurate and efficient in solving pantograph–catenary interaction dynamics with long catenary structures and can be used in hardware-in-the-loop pantograph–catenary interaction simulation.

It can be seen from these methods that the EVA is the basement of these methods, and the length of the EVA can directly decide the accuracy and efficiency of these methods. If the length of EVA is too short, the vibration of the catenary caused by the pantograph–catenary interaction cannot be fully included in the model, and its calculation accuracy is decreased. If the length of EVA is too long, the length of the catenary model is also long, and the DOFs of the model are increased, which further decreases the calculation efficiency of these new methods. Xu et al. [25] investigated the influence of the length of EVA on the calculation accuracy of the reduced catenary model and gave the proper length of EVA of a certain pantograph–catenary interaction case. However, while the length of EVA is considered in the existing literature, the way to calculate the length of EVA and the influence of different

key parameters on the length of EVA is not considered so far. This limits the application of the new efficient pantograph–catenary interaction model based on the EVA. Therefore, to better understand the basic theory of these new models and apply them in different pantograph–catenary interaction cases, it is necessary to investigate the length of EVA in the pantograph–catenary system and decide them before using the new models based on the EVA.

In this work, the length of EVA in the pantograph–catenary system is investigated. Based on the existing model developed in [26], a pantograph–catenary interaction model with a long catenary structure (30 spans) is developed, where the whole model is validated by the EN50318:2018 standard. Then, a new method is developed based on the energy distribution to obtain the length of the EVA in the pantograph–catenary interaction system. Based on this new method, the length of EVA under the influence of different contact wire tensions and vehicle velocities is investigated. The appropriate length of EVA with respect to different vehicle velocities and contact wire tensions is obtained. Finally, the real-time catenary model is used to calculate the dynamic responses of the pantograph–catenary interaction under different lengths of EVA, and the results are compared with those from measurement data to validate the obtained appropriate length of EVA. The present research results enhance the theory of the new efficient pantograph–catenary interaction models based on EVA and can be used as a supplement to these models. The rest of this paper is organized as follows. The MSM-based pantograph–catenary model and the new method to obtain the length of the EVA are described in Section 2, and the present pantograph–catenary model is validated in Section 3. The length of EVA under different conditions is calculated and validated in Section 4. Some useful conclusions based on the study are drawn in Section 5.

2. Formulation of the Pantograph–Catenary Interaction System and Length of EVA

Based on the existing MSM-based pantograph–catenary interaction model developed by Zhang et al. [26], a pantograph–catenary interaction model is formulated, and a method is developed to calculate the length of EVA, as shown in Figure 2. The stitched catenary is further considered, and the stitched wire is simplified as two spring-damping elements attached to the messenger wire at specific locations. The displacements and rotations of the reduced catenary model are assumed to be small.

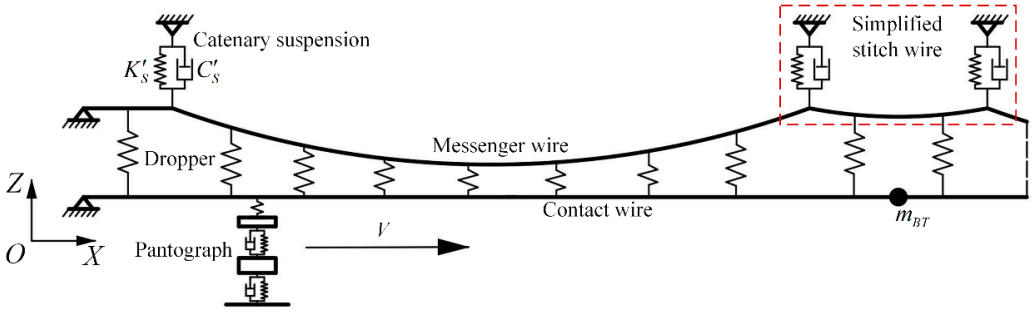

Figure 2. Model of the pantograph–catenary interaction system.

2.1. Model of the Catenary System

The catenary system is modeled based on the stitched catenary system, which mainly consists of messenger wire, contact wire, droppers, catenary suspensions, stitch wires, and registration arms. First, the contact wire and messenger wire are considered Euler—Bernoulli beams [26], with their vertical, lateral, and torsional motions considered. Based on the MSM, the kinematic energy of the contact wire and messenger wire can be expressed as

$$T_m = \frac{1}{2}\int_0^L \rho_m A_m \dot{y}_m^2 dx + \frac{1}{2}\int_0^L \rho_m A_m \dot{z}_m^2 dx + \frac{1}{2}\int_0^L \rho_m \left(I_{ym} + I_{zm}\right)\dot{\phi}_m^2 dx \quad (1)$$

$$T_c = \frac{1}{2}\int_0^L \rho_c A_c \dot{y}_c^2 dx + \frac{1}{2}\int_0^L \rho_c A_c \dot{z}_c^2 dx + \frac{1}{2}\int_0^L \rho_c \left(I_{yc} + I_{zc}\right)\dot{\phi}_c^2 dx \tag{2}$$

where the subscripts m and c correspond to the messenger and contact wire, respectively. L is the length of the catenary model, and y, z, and ϕ are the vertical, lateral, and torsional motions of the wire cross-section, respectively. ρ is the density of the beam, and A is the cross-sectional area of the wire. I_y and I_z are the second moments of the wire cross-section. The overdot on y, z, and ϕ means the time derivative of these motions. Similarly, the strain energies of the messenger and contact wire can be expressed as:

$$\begin{aligned} U_m = {} & \frac{1}{2}\int_0^L E_m I_{ym}\left(z_m''\right)^2 dx + \frac{1}{2}\int_0^L E_m I_{zm}\left(y_m''\right)^2 dx + \frac{1}{2}\int_0^L G_m I_{pm}\left(\phi_m''\right)^2 dx \\ & + \frac{1}{2}\int_0^L T_{sm}(y_m')^2 dx + \frac{1}{2}\int_0^L T_{sm}(z_m')^2 dx \end{aligned} \tag{3}$$

$$\begin{aligned} U_c = {} & \frac{1}{2}\int_0^L E_c I_{yc}\left(z_c''\right)^2 dx + \frac{1}{2}\int_0^L E_c I_{zc}\left(y_c''\right)^2 dx + \frac{1}{2}\int_0^L G_c I_{pc}\left(\phi_c''\right)^2 dx \\ & + \frac{1}{2}\int_0^L T_{sc}(y_c')^2 dx + \frac{1}{2}\int_0^L T_{sc}(z_c')^2 dx \end{aligned} \tag{4}$$

where E and G are the Young's modulus and shear modulus of the wire material, respectively. T_s is the tension of the wire. $(\cdot)'$ denotes the partial derivative of a variable $(\cdot)$ with respect to coordinate x.

Based on the Galerkin method, the displacement and rotations of the messenger and contact wire in Equations (1)–(4) can be further expressed as:

$$y_m(x,t) = \mathbf{Y}_m(x)\mathbf{q}_{my}(t),\ z_m(x,t) = \mathbf{Z}_m(x)\mathbf{q}_{mz}(t),\ \phi_m(x,t) = \mathbf{\Phi}_m(x)\mathbf{q}_{\theta mx}(t) \tag{5}$$

$$y_c(x,t) = \mathbf{Y}_c(x)\mathbf{q}_{cy}(t),\ z_c(x,t) = \mathbf{Z}_c(x)\mathbf{q}_{cz}(t),\ \phi_c(x,t) = \mathbf{\Phi}_c(x)\mathbf{q}_{\theta cx}(t) \tag{6}$$

where $\mathbf{Y}$, $\mathbf{Z}$, and $\mathbf{\Phi}$ are trial functions, and $\mathbf{q}_y$, $\mathbf{q}_z$, and $\mathbf{q}_\theta$ are the vectors of the corresponding generalized coordinates. In the present model, the boundary conditions of the messenger and contact wire are considered as simply supported, and the expressions of $\mathbf{Y}$, $\mathbf{Z}$, and $\mathbf{\Phi}$ can be seen in [26]. Based on Equations (5) and (6), in Equations (1)–(4), there are:

$$\dot{y}_m = \mathbf{Y}_m\dot{\mathbf{q}}_{my},\ \dot{z}_m = \mathbf{Z}_m\dot{\mathbf{q}}_{mz},\ \dot{\phi}_m = \mathbf{\Phi}_m\dot{\mathbf{q}}_{my},\ \dot{y}_c = \mathbf{Y}_c\dot{\mathbf{q}}_{cy},\ \dot{z}_c = \mathbf{Z}_c\dot{\mathbf{q}}_{cz},\ \dot{\phi}_c = \mathbf{\Phi}_c\dot{\mathbf{q}}_{cy} \tag{7}$$

$$y_m' = \mathbf{Y}_m'\mathbf{q}_{my},\ Z_m' = \mathbf{Z}_m'\mathbf{q}_{mz},\ \phi_m' = \mathbf{\Phi}_m'\mathbf{q}_{my},\ y_c' = \mathbf{Y}_c'\mathbf{q}_{cy},\ z_c' = \mathbf{Z}_c'\mathbf{q}_{cz},\ \phi_c' = \mathbf{\Phi}_c'\mathbf{q}_{cy} \tag{8}$$

Substituting Equations (7) and (8) into Equations (1)–(4) and using Lagrange's equation, the dynamic equations of the messenger and contact wire can be expressed as:

$$\mathbf{M}_m\ddot{\mathbf{q}}_m + \mathbf{C}_m\dot{\mathbf{q}}_m + \mathbf{K}_m\mathbf{q}_m = \mathbf{Q}_{Fm} \tag{9}$$

$$\mathbf{M}_c\ddot{\mathbf{q}}_c + \mathbf{C}_c\dot{\mathbf{q}}_c + \mathbf{K}_c\mathbf{q}_c = \mathbf{Q}_{Fc} \tag{10}$$

where $\mathbf{M}$, $\mathbf{C}$, and $\mathbf{K}$ are the mass, damping and stiffness matrices of the contact and messenger wire, respectively. $\mathbf{Q}_{Fm}$ is caused by the vertical dropper forces F_{di}, catenary suspension forces and messenger wire gravity. $\mathbf{Q}_{Fc}$ is caused by the vertical dropper forces F_{di}, registration arms gravity, and contact wire gravity. The static shape of the catenary is obtained based on its design parameters, such as the sag distance [27], and the corresponding generalized coordinate vectors $\mathbf{q}_{ms}$ and $\mathbf{q}_{cs}$ with respect to the static shape of the catenary are considered the initial conditions of Equations (9) and (10). The

derivation process of $\mathbf{Q}_F$ is the same as that shown in [24]. In Equations (9) and (10), $\mathbf{q}_m = \left[\mathbf{q}_{my}, \mathbf{q}_{mz}, \mathbf{q}_{\theta mx}\right]^T$, and $\mathbf{q}_c = \left[\mathbf{q}_{cy}, \mathbf{q}_{cz}, \mathbf{q}_{\theta cx}\right]^T$. The expressions of $\mathbf{M}_m$ and $\mathbf{K}_m$ are:

$$\mathbf{M}_m = \begin{bmatrix} \rho_m A_m \int_0^L \left(\mathbf{Y}_m^T \mathbf{Y}_m\right) dx & & \\ & \rho_m A_m \int_0^L \left(\mathbf{Z}_m^T \mathbf{Z}_m\right) dx & \\ & & \rho_m \left(I_{ym} + I_{zm}\right) \int_0^L \left(\mathbf{\Phi}_m^T \mathbf{\Phi}_m\right) dx \end{bmatrix} \tag{11}$$

$$\mathbf{K}_m = \begin{bmatrix} E_m I_{mz} \int_0^L \left(\mathbf{Y}_m''^T \mathbf{Y}_m''\right) dx & & \\ + T_{sm} \int_0^L \left(\mathbf{Y}_m'^T \mathbf{Y}_m'\right) dx & & \\ & E_m I_{my} \int_0^L \left(\mathbf{Z}_m''^T \mathbf{Z}_m''\right) dx & \\ & + T_s \int_0^L \left(\mathbf{Z}_m'^T \mathbf{Z}_m'\right) dx & \\ & & G_m I_{pm} \int_0^L \left(\mathbf{\Phi}_m'^T \mathbf{\Phi}_m'\right) dx \end{bmatrix} \tag{12}$$

Based on the Rayleigh damping theory, $\mathbf{C}_m = \alpha \mathbf{M}_m + \beta \mathbf{K}_m$, where $\alpha = \beta = 0.02$. Similarly, the expressions of $\mathbf{M}_c$ and $\mathbf{K}_c$ are:

$$\mathbf{M}_c = \begin{bmatrix} \rho_c A_c \int_0^l \left(\mathbf{Y}_c^T \mathbf{Y}_c\right) dx & & \\ & \rho_c A_c \int_0^l \left(\mathbf{Z}_c^T \mathbf{Z}_c\right) dx & \\ & & \rho_c \left(I_{yc} + I_{zc}\right) \int_0^l \left(\mathbf{\Phi}_c^T \mathbf{\Phi}_c\right) dx \end{bmatrix} \tag{13}$$

$$\mathbf{K}_c = \begin{bmatrix} E_c I_{cz} \int_0^L \left(\mathbf{Y}_c''^T \mathbf{Y}_c''\right) dx & & \\ + T_{sc} \int_0^L \left(\mathbf{Y}_c'^T \mathbf{Y}_c'\right) dx & & \\ & E_c I_{cy} \int_0^L \left(\mathbf{Z}_c''^T \mathbf{Z}_c''\right) dx & \\ & + T_{sc} \int_0^L \left(\mathbf{Z}_c'^T \mathbf{Z}_c'\right) dx & \\ & & G_c I_{pc} \int_0^L \left(\mathbf{\Phi}_c'^T \mathbf{\Phi}_c'\right) dx \end{bmatrix} \tag{14}$$

and $\mathbf{C}_c = \alpha \mathbf{M}_c + \beta \mathbf{K}_c$.

The droppers, catenary suspension, stitch wire, and registration arm are then modeled. The droppers are modeled as a bilinear spring element with zero stiffness in compression, and the dropper forces are calculated as:

$$F_{di} = \begin{cases} (d_{ci} - d_{mi}) k_{id}, & d_{ci} - d_{mi} \geq 0 \\ 0, & d_{ci} - d_{mi} < 0 \end{cases}, \tag{15}$$

where k_{id} is the ith dropper stiffness and d_{ci} and d_{mi} are the displacements of the contact wire and messenger wire at the dropper-connected locations based on the static shape of the catenary. The static force of every dropper should also be considered in the calculation process. The suspension of the catenary is modeled as spring-damper elements with stiffness K_s' and damping C_s'. The registration arm is modeled as a lumped mass m_{BT} attached to the contact wire.

As mentioned above, the stitch wire is simplified as two spring-damping elements attached to the messenger wire at the stitch wire location. The stiffness and damping of these two spring-damping elements should be calculated based on the stiffness and damping of the catenary suspension and dropper.

2.2. Pantograph Model

The pantograph is then modeled as a lumped mass model [27], as shown in Figure 2. These lumped masses are connected with each other through spring-damper elements. The mass, stiffness, and damping of these lumped mass and spring-damper elements should

be chosen to let the frequency of the model be equal to those of different real pantographs. The dynamic equation of the pantograph is:

$$\mathbf{M}_P\ddot{\mathbf{q}}_P + \mathbf{C}_P\dot{\mathbf{q}}_P + \mathbf{K}_P\mathbf{q}_P = \mathbf{Q}_P \tag{16}$$

where $\mathbf{M}_P$, $\mathbf{C}_P$, and $\mathbf{K}_P$ are the spring, damping and stiffness matrices of the pantograph system, respectively. $\mathbf{q}_P$ is the generalized coordinate vector of the pantograph system. $\mathbf{Q}_P$ is the generalized force vector generated according to the pantograph gravity, uplift forces, and pantograph–catenary contact forces. The uplift force is applied on the third lumped mass m_3, and the aerodynamic force is applied on the first lumped mass m1 (pantograph head). The aerodynamic force is calculated by [28]:

$$F_{ad} = 0.0097V^2 \tag{17}$$

and the uplift force has a constant value of 70 N. Details of these matrices' expressions can be seen in [27].

2.3. Pantograph–Catenary Interaction Model

Based on the dynamic equations of the catenary and pantograph, the dynamic equations of the whole pantograph–catenary interaction model can be expressed as:

$$\begin{bmatrix} \mathbf{M}_m & & \\ & \mathbf{M}_c & \\ & & \mathbf{M}_P \end{bmatrix} \begin{bmatrix} \ddot{\mathbf{q}}_m \\ \ddot{\mathbf{q}}_c \\ \ddot{\mathbf{q}}_P \end{bmatrix} + \begin{bmatrix} \mathbf{C}_m & & \\ & \mathbf{C}_c & \\ & & \mathbf{C}_P \end{bmatrix} \begin{bmatrix} \dot{\mathbf{q}}_m \\ \dot{\mathbf{q}}_c \\ \dot{\mathbf{q}}_P \end{bmatrix} + \begin{bmatrix} \mathbf{K}_m & & \\ & \mathbf{K}_c & \\ & & \mathbf{K}_P \end{bmatrix} \begin{bmatrix} \dot{\mathbf{q}}_m \\ \dot{\mathbf{q}}_c \\ \dot{\mathbf{q}}_P \end{bmatrix} = \begin{bmatrix} \mathbf{Q}_{Fm} \\ \mathbf{Q}_{Fc} \\ \mathbf{Q}_P \end{bmatrix} \tag{18}$$

In Equation (17), the pantograph–catenary contact force is calculated based on the following equation:

$$F_c = \begin{cases} k_n d_r, \ d_r \geq 0 \\ 0, \ d_r < 0 \end{cases} \tag{19}$$

where k_n is the contact stiffness and d_r is the relative distance between the contact wire and contact strip of the pantograph at the contact point. The position of the contact point changes with the movement of the pantograph. The value of k_n can be chosen as 50,000 N/m [27]. The present model is achieved in the commercial software MATLAB 2022a, and Equation (17) is solved by a variable-step, variable-order (VSVO) solver (MATLAB function ode15s).

2.4. Calculation Method of the Length of EVA

After the formulation of the pantograph–catenary interaction model, the EVA of the pantograph–catenary interaction system is determined. Note that the vibration of the catenary consists of vertical, lateral, and torsional vibrations of the contact and messenger wire, and it is difficult to present all of these results in one paper. However, the propagation of vibration can be considered as the propagation of energy, and the energy distribution of the catenary directly presents the vibration distribution situations, which is helpful in determining the EVA with most of the vibration included. Therefore, the energy distribution of the catenary is concentrated and calculated. Based on Equations (1)–(4), the vibration energy at an arbitrary location of the catenary can be calculated as:

$$\begin{aligned} E_x = {} & \tfrac{1}{2}\rho_m A_m\left(\dot{y}_{mx}^2 + \dot{z}_{mx}^2\right) + \rho_m\left(I_{ym} + I_{zm}\right)\dot{\phi}_{mx}^2 + \tfrac{1}{2}\rho_c A_c\left(\dot{y}_{cx}^2 + \dot{z}_{cx}^2\right) + \rho_c\left(I_{yc} + I_{zc}\right)\dot{\phi}_{cx}^2 \\ & + \tfrac{1}{2}E_m\left(I_{ym}\left(z''_{mx}\right)^2 + I_{zm}\left(y''_{mx}\right)^2\right) + G_m I_{pm}\left(\phi''_{mx}\right)^2 + \tfrac{1}{2}T_{sm}\left(\left(y'_{mx}\right)^2 + \left(z'_{mx}\right)^2\right) \\ & + \tfrac{1}{2}E_c\left(I_{yc}\left(z''_{cx}\right)^2 + I_{zc}\left(y''_{cx}\right)^2\right) + G_c I_{pc}\left(\phi''_{cx}\right)^2 + \tfrac{1}{2}T_{sc}\left(\left(y'_{cx}\right)^2 + \left(z'_{cx}\right)^2\right) \end{aligned} \tag{20}$$

where y_{mx}, z_{mx}, and ϕ_{mx} are the vertical, lateral, and torsional motions of the messenger wire at arbitrary location x, respectively. y_{cx}, z_{cx}, and ϕ_{cx} are the vertical, lateral, and torsional motions of the contact wire at arbitrary location x, respectively.

Based on the energy distribution of the catenary, the length of the EVA can be further decided. As mentioned above, the EVA is determined to include most of the vibration caused by the pantograph–catenary interaction. Thus, if the total energy of the EVA converges, the length of the EVA is long enough to include most of the vibration caused by the pantograph–catenary interaction. The total energy of the EVA can be calculated by:

$$E = \int_{x_p - \frac{1}{2}d_e}^{x_p + \frac{1}{2}d_e} E_x dx \tag{21}$$

where x_p is the location of the pantograph, and d_e is the length of the EVA. The convergence of total energy is defined as the difference between two neighboring values within a tolerable error of 0.01 J.

3. Validation

After the modeling of the pantograph–catenary interaction system, the present model is validated by the EN50318:2018 standard [11], where the stitched catenary and its corresponding double pantograph are considered, and the pantograph distance is 200 m. The total length of the catenary is 1800 m (30 spans), and the number of modes used in the calculation is n = 1200. Two vehicle operation velocities, V = 275 km/h and 320 km/h, are considered for simulation. The time histories of the pantograph–catenary contact force with respect to different pantographs and vehicle velocities are shown in Figure 3, and their corresponding statistical results are shown in Table 1, which are compared with those from the EN50318:2018 standard. It can be seen from Figure 3 that the calculation results from the present model are reasonable, and their corresponding statistical results show good agreement with those listed in the EN 50318-2018 standard, which means that the present model can accurately simulate the dynamic responses of the pantograph–catenary interaction in a stitched catenary system.

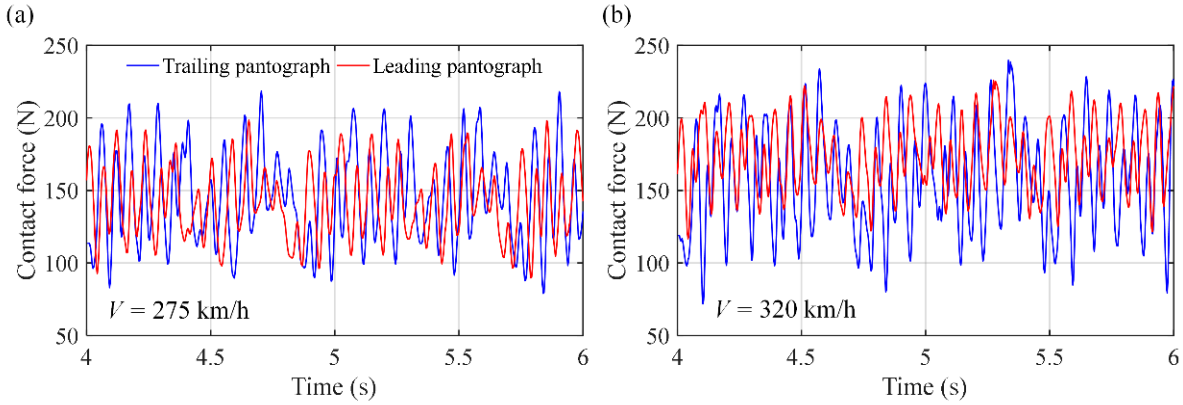

Figure 3. Time histories of pantograph–catenary contact forces with respect to different pantographs and velocities: (**a**) V = 275 km/h and (**b**) V = 320 km/h.

Table 1. Statistical results of the pantograph–catenary interaction with respect to different pantographs at V = 275 and 320 km/h and comparison with the values in EN50318:2018 (in parentheses).

Speed [km/h]	275		320	
Pantograph	Leading	Trailing	Leading	Trailing
F_m [N]	143.5 (143–144)	143.5 (142–144)	169 (169)	169 (169)
σ [N]	23.8 (20.2–14.7)	28.2 (24.4–36.2)	22.8 (20.5–24.7)	34.9 (30.4–38.3)
σ (0 Hz–5 Hz) [N]	14.2 (11.7–15.2)	17.4 (17.0–18.2)	12.8 (11.8–13.3)	22.4 (20.4–24.2)
σ (5 Hz–20 Hz) [N]	18.3 (16.5–19)	24.9 (16.4–27.4)	18.1 (15.2–20.9)	27.8 (21.5–29.8)

Table 1. *Cont.*

Actual maximum of contact force [N]	197.6 (185–199)	224.1 (203–252)	227.6 (210–232)	246.1 (239–255)
Actual minimum of contact force [N]	97.1 (92–102)	85.2 (56–88)	122.3 (105–128)	75.2 (43–78)
Range of vertical position of the point of contact [mm]	23.1 (18–25)	33.5 (26–36)	20.9 (13–23)	59.1 (38–63)
Maximum uplift at support [mm]	67.8 (55–79)	73.1 (51–79)	89.2 (74–95)	90.2 (69–95)
Percentage of loss of contact [%]	0 (0)	0 (0)	0 (0)	0 (0)

4. Study on the Length of EVA in the Pantograph–Catenary System

4.1. Influence of Different Vehicle Velocity and Contact Wire Tension on the Length of EVA

In the catenary system, the wave velocity is determined by the vehicle velocity and contact wire tension [29], and the wave velocity also influences the propagation of vibration and energy distribution. Besides, the temperature change can also influence the contact wire tension. Therefore, the influence of vehicle velocity and contact wire tension on the energy distribution of the catenary is investigated. The Sweden stitched catenary system SYT7.0/9.8 interacting with a high-speed pantograph is formulated based on the present model, and their key parameters are obtained from [27]. The energy distribution of the catenary under the influence of different vehicle velocities V is firstly calculated based on Equation (20) and shown in Figure 4, where V is chosen from 150 km/h, 222 km/h, and 250 km/h. Figure 4 shows that V has an obvious influence on the energy distribution. As V increases from 150 km/h to 222 km/h, the maximum energy increases from 0.31 J to 0.78 J, and other peaks also increase. Most importantly, the energy of those places far from the pantograph also increases. For example, the energy of the catenary at x = 18 m increases from 0.001 J to 0.24 J, which means that the vibration propagated to this place at V = 250 km/h, and the EVA should also increase to include these vibrations.

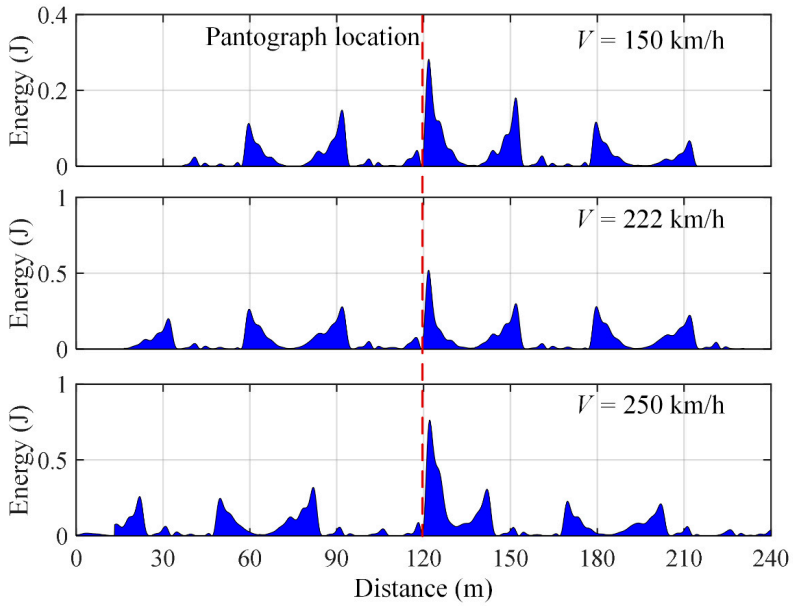

Figure 4. The energy distribution of the catenary at different vehicle velocities.

The energy distribution of the catenary under the influence of different contact wire tensions is then shown in Figure 5, where the contact wire tension changes from 9.8 kN to 15.8 kN. It can be seen from Figure 5 that the contact wire tension T_S also influences

the energy distribution, but its influence is smaller than that of the vehicle velocity. The maximum energy of the catenary decreases from 0.51 J to 0.23 J as the T_S increases from 9.8 kN to 15.8 kN, and the other peaks also decrease. However, the general shape of the energy distribution has no obvious changes, and the vibration propagation distance is reduced shortly. When T_S = 9.8 kN, the closest location with energy smaller than 0.01 J is x = 21.2 m, but it only changes to x = 25.7 m as T_S increases to 15.8 kN.

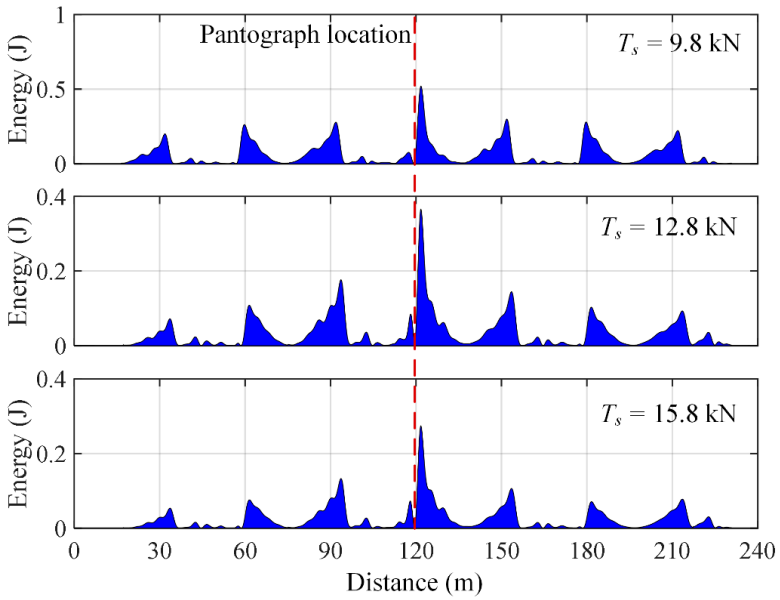

Figure 5. The energy distribution of the catenary at different contact wire tensions.

The total energy of the EVA with respect to the length of the EVA under the influence of different V and T_s is then calculated based on Equation (21), as shown in Figure 6. It can be seen from Figure 6 that the total energy of the EVA converged to different values at different V and T_s values, and its corresponding length also changes. When V = 150 km/h, the total energy of the EVA converged to 46.2 J with d_e = 185.2 m, and it further increased to 118.4 J with d_e = 257.8 m and V = 250 km/h. When TS increases from 9.8 kN to 15.8 kN, the converged total energy of the EVA decreases from 105.1 J to 52.1 J as d_e changes from 215.3 m to 186.4 m. Based on this, the appropriate length of the EVA can be clearly determined by its energy distribution.

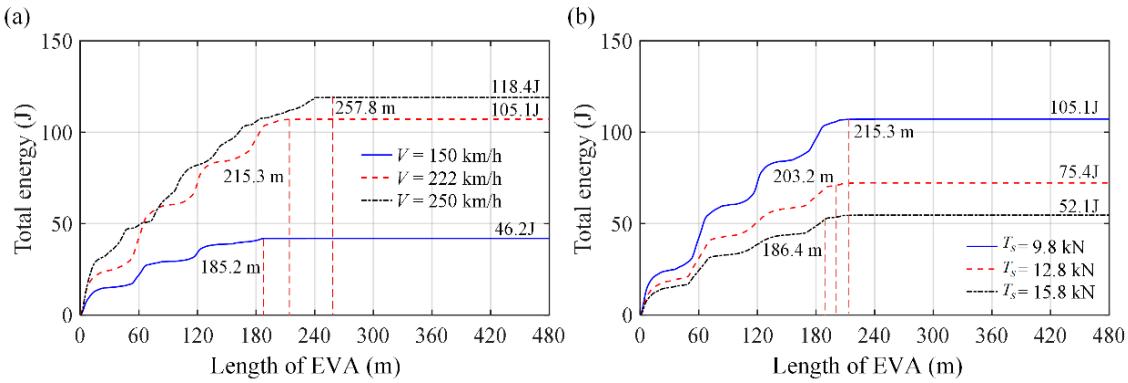

Figure 6. The total energy of the EVA with respect to different lengths under the influence of different vehicle velocities and contact wire tensions: (**a**) different vehicle velocities and (**b**) different contact wire tensions.

The appropriate length of EVA with respect to different key parameters is finally analyzed. Based on the present model, the appropriate length of EVA with respect to

different V and T_s is shown in Figure 7. Figure 7 shows that the appropriate length of EVA increases with increasing vehicle velocity but decreases with increasing contact wire tension. When V = 150 km/h and T_s = 9.8 kN, the appropriate length of EVA should be 215.2 m, and it can decrease to 186.4 m with T_s = 15.8 kN. Furthermore, when the vehicle velocity is smaller than 100 km/h and the contact wire tension is larger than 18.8 kN, the appropriate length of EVA converges to a value larger than 160 m. This means that the appropriate length of EVA should be no less than 160 m under different situations in the present pantograph–catenary interaction system.

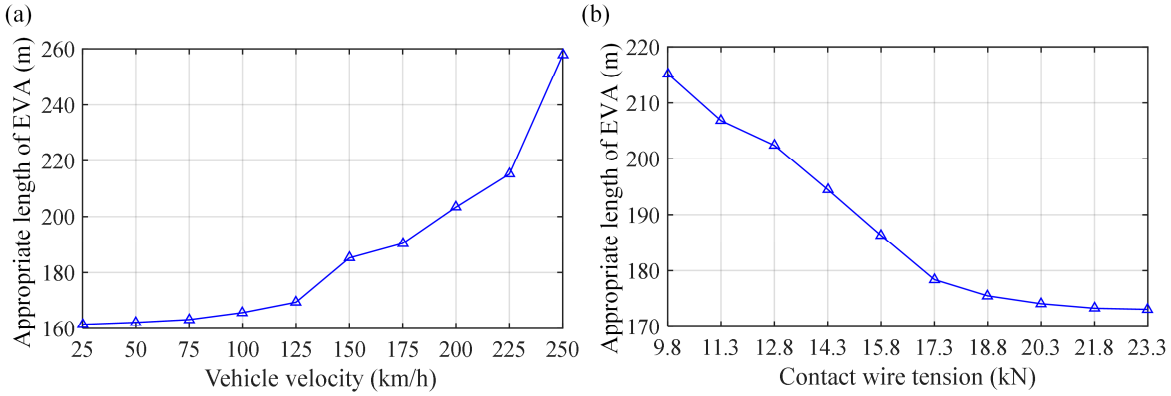

Figure 7. Appropriate length of EVA with respect to different key parameters: (**a**) vehicle velocity and (**b**) contact wire tension.

4.2. Influence of the EVA Length on the Real-Time Catenary Model Calculation Accuracy

In this section, the existing real-time catenary model [18] is further considered to study the influence of the EVA length on its calculation accuracy and validate the appropriate length of EVA. The abovementioned pantograph–catenary system is further considered, and the corresponding pantograph–catenary contact force is calculated. The measurement data of the contact force obtained from [27] are used for validation purposes. Both the calculation results and measurement data are filtered in a 0–20 Hz span. Based on the test parameters, the train velocity is chosen as 222 km/h. Four different EVA lengths are chosen, which are 60 m, 120 m, 240 m, and an appropriate length of 215 m, and the EVA length is equal to the length of the real-time catenary model. The time histories of the contact force of the pantograph–catenary system are shown in Figure 8. It can be seen from Figure 8 that the length of the EVA has a great influence on the pantograph–catenary interaction dynamics. When d_e = 60 m and 120 m, the results from the real-time catenary model show a large difference between the measurement data. However, when the appropriate length of 215 m is chosen, the results from the real-time catenary model show good agreement with the measurement data. This means that the real-time catenary model can obtain accurate results with an appropriate length of EVA, and the appropriate length of EVA can be obtained based on the energy distribution of the catenary. In addition, it can be seen from Figure 8d that an EVA length longer than its appropriate value can also obtain accurate results.

The mean contact force and standard deviation of the pantograph–catenary contact force with respect to different lengths of EVA are further calculated to validate the appropriate length of EVA, as shown in Figure 9, where the results are compared with those from the test results. Note that the minimum contact force of the test results cannot be fully consistent with those from the real-time catenary model; thus, it is not considered for validation. Figure 9 shows that the results from the real-time catenary model become closer to those from the test results with increasing EVA length. When the length of EVA becomes 210 m and higher, the mean contact force converges to 85.8 N, and the standard deviation converges to 18.9 N. Because these two values of the test results are 85.1 N and 18.2 N, the maximum relative difference between these results is not more than 1%. Based on

this, the appropriate length of EVA can allow accurate results to be obtained in a real-time catenary model.

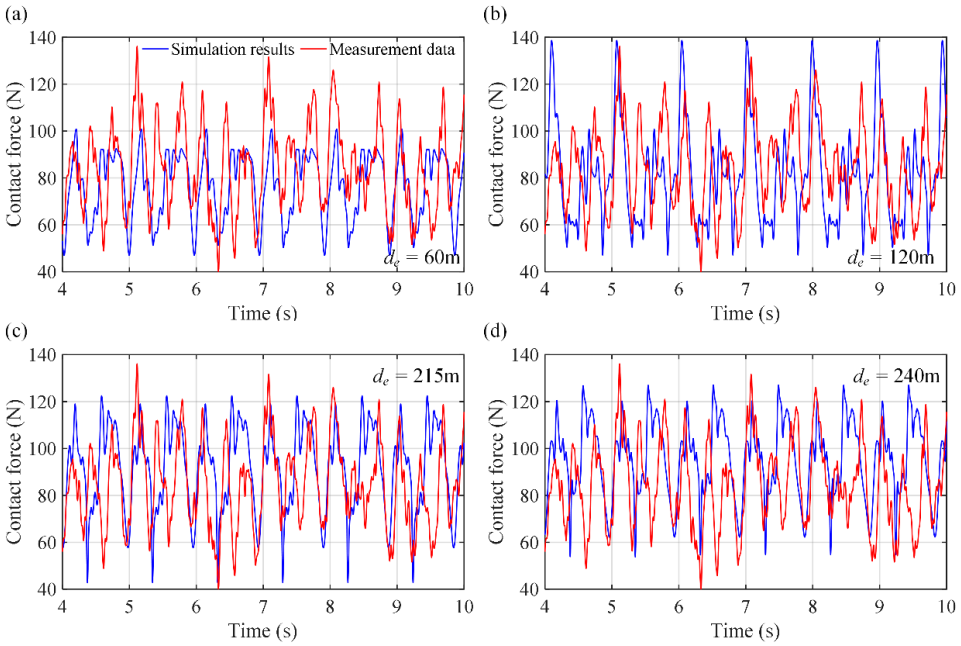

Figure 8. Time histories of the pantograph–catenary contact force at V = 222 km/h with respect to different lengths of EVA d_e: (**a**) d_e = 60 m; (**b**) d_e = 120 m; (**c**) d_e = 215 m and (**d**) d_e = 240 m.

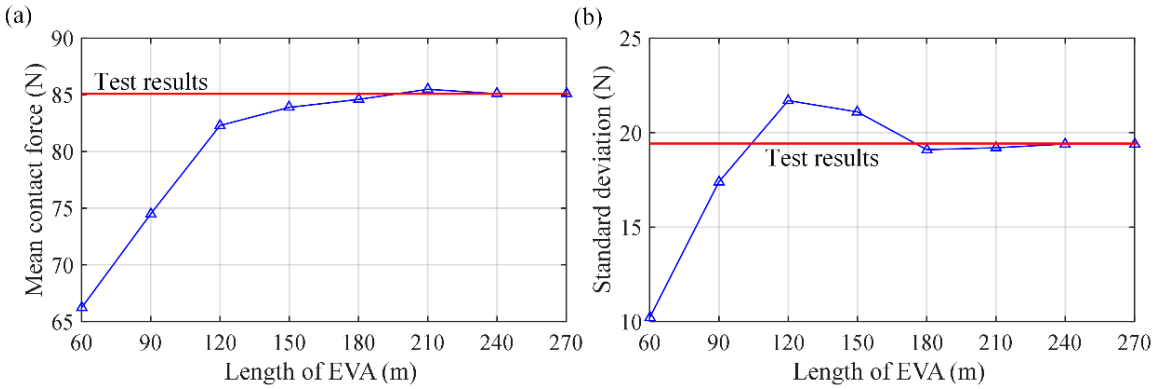

Figure 9. Mean contact force and standard deviation of the pantograph–catenary contact force with respect to different lengths of EVA: (**a**) Mean contact force and (**b**) standard deviation.

5. Conclusions

The effective vibration area (EVA) includes most of the catenary vibration caused by pantograph–catenary interactions and is the basis of the real-time catenary model for hardware-in-loop simulation. However, while the length of EVA can directly influence the calculation accuracy and efficiency of the real-time catenary model, the way to calculate the length of EVA and the influence of different key parameters on the length of EVA is not considered so far. In this work, the length of EVA in the pantograph–catenary system is investigated. Based on a pantograph–catenary interaction system, a new method is developed based on the energy distribution to obtain the length of the effective vibration area (EVA) of the catenary in the pantograph–catenary interaction system. Then, the length of EVA under the influence of different contact wire tensions and vehicle velocities is investigated. The appropriate length of EVA with respect to different vehicle velocities and contact wire tensions is obtained. The real-time catenary model is used to calculate the dynamic responses of the pantograph–catenary interaction under different lengths of EVA, and the results are compared with those from measurement data to validate the

obtained appropriate length of EVA. The present research results enhance the theory of the new efficient pantograph–catenary interaction models based on EVA and can be used as a supplement to these models.

Based on the investigation results, the following conclusions are drawn:

(1) The present methods can obtain the appropriate length of EVA in the pantograph–catenary system. The length of the EVA corresponding to the converged total energy obtains accurate results in the real-time catenary model. Therefore, it is suggested to use the present method to obtain an appropriate length of EVA before using the real-time catenary model and other similar methods with different kinds of pantograph–catenary interaction systems considered.

(2) The length of the EVA is greatly influenced by the vehicle velocity and contact wire tension. The appropriate length of EVA increases with increasing vehicle velocity and decreases with increasing contact wire tension. Based on the calculation results, the appropriate length of EVA should be no less than 160 m under different situations. This value can be used as a reference for the real-time catenary model and other similar methods based on the EVA.

In the present work, a specific experiment to validate and investigate the length of EVA in the pantograph–catenary system under different conditions is not considered due to the limitation of time and funds. In the next work, a new experiment will be conducted to investigate the length of EVA in the pantograph catenary system under different conditions, especially the influence of wind and ice.

Author Contributions: Methodology, L.C.; Software, L.P. and Y.X.; Validation, L.C., L.P. and C.H.; Formal analysis, Y.X.; Data curation, C.H.; Writing—original draft, L.C.; Writing—review & editing, L.P. and Y.X. All authors have read and agreed to the published version of the manuscript.

Funding: This work is supported by the Research Project of China Academy of Railway Sciences Group Co., Ltd. (Grant No. 2023YJ271), China Railway Group (Grant No. N2023G065) and the National Natural Science Foundation of China (grant number 12302048).

Institutional Review Board Statement: Not applicable.

Informed Consent Statement: Not applicable.

Data Availability Statement: The raw data supporting the conclusions of this article will be made available by the authors on request.

Conflicts of Interest: Authors Liming Chen and Like Pan were employed by the company China Academy of Railway Sciences Co., Ltd. The remaining authors declare that the research was conducted in the absence of any commercial or financial relationships that could be construed as a potential conflict of interest. The authors declare that this study received funding from China Academy of Railway Sciences Group Co., Ltd. and China Railway Group. The funder was not involved in the study design, collection, analysis, interpretation of data, the writing of this article or the decision to submit it for publication.

References

1. Zhu, G.Y.; Gao, G.Q.; Wu, G.N.; Gu, Z.; Wu, J.; Hao, J. Modeling pantograph-catenary arcing. *Proc. Inst. Mech. Eng. F J. Rail Rapid Transit* **2016**, *230*, 1687–1697. [CrossRef]
2. Bucca, G.; Collina, A. A procedure for the wear prediction of collector strip and contact wire in pantograph-catenary system. *Wear* **2009**, *266*, 46–59. [CrossRef]
3. Song, Y.; Duan, F.; Liu, Z. Analysis of Critical Speed for High-Speed Railway Pantograph-Catenary System. *IEEE Trans. Veh. Technol.* **2022**, *71*, 3547–3555. [CrossRef]
4. Wang, Y.; Liu, Z.; Mu, X.; Huang, K.; Wang, H.; Gao, S. An Extended Habedank's Equation-Based EMTP Model of Pantograph Arcing Considering Pantograph-Catenary Interactions and Train Speeds. *IEEE Trans. Power Deliv.* **2016**, *31*, 1186–1194. [CrossRef]
5. Poetsch, G.; Evans, J.; Meisinger, R.; Kortüm, W.; Baldauf, W.; Veitl, A.; Wallaschek, J. Pantograph/catenary dynamics and control. *Veh. Syst. Dyn.* **1997**, *28*, 159–195. [CrossRef]
6. Zhang, W.; Mei, G.; Zeng, J. A study of pantograph/catenary system dynamics with influence of presag and irregularity of contact wire. *Veh. Syst. Dyn.* **2002**, *37*, 593–604. [CrossRef]

7. Bocciolone, M.; Resta, F.; Rocchi, D.; Tosi, A.; Collina, A. Pantograph aerodynamic effects on the pantograph-catenary interaction. *Veh. Syst. Dyn.* **2006**, *44*, 560–570. [CrossRef]
8. Gregori, S.; Tur, M.; Nadal, E.; Aguado, J.; Fuenmayor, F.; Chinesta, F. Fast simulation of the pantograph–catenary dynamic interaction. *Finite Elem. Anal. Des.* **2017**, *129*, 1–13. [CrossRef]
9. Wu, T.X.; Brennan, M.J. Basic analytical study of pantograph-catenary system dynamics. *Veh. Syst. Dyn.* **1998**, *30*, 443–456. [CrossRef]
10. Bruni, S.; Ambrosio, J.; Carnicero, A.; Cho, Y.H.; Finner, L.; Ikeda, M.; Kwon, S.Y.; Massat, J.-P.; Stichel, S.; Tur, M.; et al. The results of the pantograph-catenary interaction benchmark. *Veh. Syst. Dyn.* **2015**, *53*, 412–435. [CrossRef]
11. *EN 50318*; Railway Applications—Current Collection Systems—Validation of Simulation of the Dynamic Interaction between Pantograph and Overhead Contact Line. European Committee for Electrotechnical Standardization: Brussels, Belgium, 2018. Available online: https://www.en-standard.eu/bs-en-50318-2018-a1-2022-railway-applications-current-collection-systems-validation-of-simulation-of-the-dynamic-interaction-between-pantograph-and-overhead-contact-line/ (accessed on 1 July 2024).
12. Song, Y.; Wang, H.; Frøseth, G.; Nåvik, P.; Liu, Z.; Rønnquist, A. Surrogate modelling of railway pantograph-catenary interaction using deep Long-Short-Term-Memory neural networks. *Mech. Mach. Theory* **2023**, *187*, 105386. [CrossRef]
13. Song, Y.; Zhang, M.; Øiseth, O.; Rønnquist, A. Wind deflection analysis of railway catenary under crosswind based on nonlinear finite element model and wind tunnel test. *Mech. Mach. Theory* **2022**, *168*, 104608. [CrossRef]
14. Massat, J.-P.; Laurent, C.; Bianchi, J.-P.; Balmès, E. Pantograph catenary dynamic optimisation based on advanced multibody and finite element co-simulation tools. *Veh. Syst. Dyn.* **2014**, *52*, 338–354. [CrossRef]
15. Tur, M.; García, E.; Baeza, L.; Fuenmayor, F. A 3D absolute nodal coordinate finite element model to compute the initial configuration of a railway catenary. *Eng. Struct.* **2014**, *71*, 234–243. [CrossRef]
16. Nåvik, P.; Rønnquist, A.; Stichel, S. Identification of system damping in railway catenary wire systems from full-scale measurements. *Eng. Struct.* **2016**, *113*, 71–78. [CrossRef]
17. Rønnquist, A.; Nåvik, P. Dynamic assessment of existing soft catenary systems using modal analysis to explore higher train velocities: A case study of a Norwegian contact line system. *Veh. Syst. Dyn.* **2015**, *53*, 756–774. [CrossRef]
18. Facchinetti, A.; Bruni, S. Hardware-in-the-loop hybrid simulation of pantographcatenary interaction. *J. Sound Vib.* **2012**, *331*, 2783–2797. [CrossRef]
19. Bruni, S.; Bucca, G.; Collina, A.; Facchinetti, A. Numerical and hardware-in-the-loop tools for the design of very high speed pantograph-catenary systems. *J. Comput. Nonlinear Dyn.* **2012**, *7*, 041013. [CrossRef]
20. Facchinetti, A.; Gasparetto, L.; Bruni, S. Real-time catenary models for the hardware-in-The-loop simulation of the pantograph-catenary interaction. *Veh. Syst. Dyn.* **2013**, *51*, 499–516. [CrossRef]
21. Cao, T.N.T.; Reddy, J.; Ang, K.K.; Luong, V.H.; Tran, M.T.; Dai, J. Dynamic analysis of three-dimensional high-speed train-track model using moving element method. *Adv. Struct. Eng.* **2018**, *21*, 862–876. [CrossRef]
22. Koh, C.G.; Ong, J.S.Y.; Chua, D.K.H.; Feng, J. Moving element method for train-track dynamics. *Int. J. Numer. Methods Eng.* **2003**, *56*, 1549–1567. [CrossRef]
23. Xu, Y.; Zhu, W.; Fan, W.; Yang, C.; Zhang, W. A new three-dimensional moving timoshenko beam element for moving load problem analysis. *J. Vib. Acoust. Trans. ASME* **2020**, *142*, 1–39. [CrossRef]
24. Yang, C.; Xu, Y.; Zhu, W.; Fan, W.; Zhang, W.; Mei, G. A three-dimensional modal theory-based Timoshenko finite length beam model for train-track dynamic analysis. *J. Sound Vib.* **2020**, *479*, 115363. [CrossRef]
25. Xu, Y.; Liu, Z.D.; Stichel, S.; Zhu, W.D.; Lei, J.L.; Yao, Y. A comparative study on the influence of typical track failures on high-speed pantograph-catenary interaction dynamics. *Veh. Syst. Dyn.* **2024**, 1–29. [CrossRef]
26. Zhang, W.; Liu, Y.; Mei, G. Evaluation of the coupled dynamical response of a pantograph—Catenary system: Contact force and stresses. *Veh. Syst. Dyn.* **2006**, *44*, 645–658. [CrossRef]
27. Liu, Z.; Jönsson, P.-A.; Stichel, S.; Rønnquist, A. Implications of the operation of multiple pantographs on the soft catenary systems in Sweden. *Proc. Inst. Mech. Eng. F J. Rail Rapid Transit* **2016**, *230*, 971–983. [CrossRef]
28. *EN50367*; A Railway Applications-Current Collection System-Technical Criteria for the Interaction between Pantograph and Overhead Line. CENELEC: Brussels, Belgium, 2006. Available online: https://www.en-standard.eu/bs-en-50367-2020-a1-2022-railway-applications-fixed-installations-and-rolling-stock-criteria-to-achieve-technical-compatibility-between-pantographs-and-overhead-contact-line/ (accessed on 1 July 2024).
29. Vesali, F.; Rezvani, M.A.; Molatefi, H. Analysis of conceptual similarities and differences of wave speed and critical speed in the overhead catenary system. *Measurement* **2021**, *176*, 109164. [CrossRef]